Cerebral Cortex, 2020;32: 2745–2761

https://doi.org/10.1093/cercor/bhab378
Advance Access Publication Date: 4 November 2021
Original Article

ORIGINAL ARTICLE

Prefrontal Control of Proactive and Reactive Mechanisms of Visual Suppression

Fabio Di Bello[1,2], Sameh Ben Hadj Hassen[1], Elaine Astrand[1,3] and Suliann Ben Hamed[1]

[1]Institut des Sciences Cognitives Marc Jeannerod, CNRS, UMR5229, 69675 Bron Cedex, France, [2]Department of Physiology and Pharmacology, Sapienza University of Rome, 00185 Rome, Italy and [3]School of Innovation, Design, and Engineering, Mälardalen University, IDT, 721 23 Västerås, Sweden

Address correspondence to Fabio Di Bello. Email: fab.dibello@gmail.com; Suliann Ben Hadj Hamed. Email: benhamed@isc.cnrs.fr

Abstract

In everyday life, we are continuously struggling at focusing on our current goals while at the same time avoiding distractions. Attention is the neuro-cognitive process devoted to the selection of behaviorally relevant sensory information while at the same time preventing distraction by irrelevant information. Distraction can be prevented proactively, by strategically prioritizing task-relevant information at the expense of irrelevant information, or reactively, by suppressing the ongoing processing of distractors. The distinctive neuronal signature of these suppressive mechanisms is still largely unknown. Thanks to machine-learning decoding methods applied to prefrontal cortical activity, we monitor the dynamic spatial attention with an unprecedented spatial and temporal resolution. We first identify independent behavioral and neuronal signatures for long-term (learning-based spatial prioritization) and short-term (dynamic spatial attention) mechanisms. We then identify distinct behavioral and neuronal signatures for proactive and reactive suppression mechanisms. We find that while distracting task-relevant information is suppressed proactively, task-irrelevant information is suppressed reactively. Critically, we show that distractor suppression, whether proactive or reactive, strongly depends on the implementation of both long-term and short-term mechanisms of selection. Overall, we provide a unified neuro-cognitive framework describing how the prefrontal cortex deals with distractors in order to flexibly optimize behavior in dynamic environments.

Key words: attention, attention selection, attentional spotlight, distractor suppression, prefrontal cortex, priority map, proactive suppression, reactive suppression

Introduction

Focusing on current behavioral goals while at the same time avoiding distraction is critical for survival. Attention is the neuro-cognitive system devoted to the filtering of incoming information so that behaviorally relevant events are selected at the expense of behaviorally irrelevant events and distractors. Subjects accomplish this task by leveraging selective and suppressive attentional mechanisms, the effect of which is to optimize visual resources to ongoing behavioral demands and environmental constraints. The top-down selection of visual information takes place through two distinct mechanisms (Baluch and Itti 2011; Gilbert and Li 2013; Nobre and Kastner 2014; Moore and Zirnsak 2017). Task-relevant items can be prioritized because subjects have learned the specific contingencies of the ongoing task, resulting in a biased processing of relevant task items relative to irrelevant task items, and defining a so-called spatial priority map (Desimone and Duncan 1995; Chelazzi et al. 2014; Li et al. 2018). Task-relevant items can also be prioritized by a voluntary allocation of the attentional spotlight (Posner 1980; Doricchi et al. 2009; Di Bello et al. 2019).

Growing evidence indicate that this latter prioritization is highly dynamic in time and space (Landau and Fries 2012; Fiebelkorn et al. 2013, 2018; Astrand et al. 2016; Fiebelkorn and Kastner 2019; Gaillard et al. 2020). This voluntary allocation of attention, also referred to as covert or endogenous attention, depends on the spur of the moment and contrasts with the learning-based spatial prioritization that operates on a larger time scale (Leber 2010). It is hypothesized that both these attentional processes share the same neuronal substrates.

On the other hand, subjects cope with distractors by implementing both proactive and reactive mechanisms of suppression. Proactive suppression is mainly conceived as a consequence of the top-down control of these two described attentional selective mechanisms. For instance, the allocation of the (long- and short-term) attentional resources toward the expected task-relevant information also involves the suppression of the irrelevant stimuli, suggesting a unique push-pull selection/suppression mechanism (see Chelazzi et al. 2019 for an extended review). However, in daily life, irrelevant stimuli still often succeed in capturing our attention and our visual resources. In such eventuality situation, the reactive suppression of their visual processing and the related decision-making processes needs to be implemented in order to interrupt inappropriate responses. Despite proactive and reactive mechanisms of suppression being well established from a behavioral point of view (Geng 2014; Marini et al. 2016), the environmental circumstances favoring the implementation of one or the other are still unknown. For example, it is not clear if the steady allocation of the attentional resources that underlies proactive suppression corresponds to the same mechanisms as the attentional disengagement that characterizes reactive rejections.

Mirroring this state of the art, the neuronal correlates underlying proactive and reactive mechanisms of visual suppression are still largely debated (Hickey et al. 2009; Marini et al. 2016; Vissers et al. 2016; Perri 2019). Preliminary studies indicate that while proactive strategies are mainly implemented by a general sustained activity in the fronto-parietal attention network (Corbetta et al. 2008; Demeter et al. 2011), reactive mechanisms are related to the activation of the medio-frontal and insular cortex (Durston et al. 2003; Wager et al. 2005). However, it has been also suggested that these two types of suppression may share, at least partially, common neural substrates (Marini et al. 2016; Cosman et al. 2018; Perri 2019). Frontal eye field (FEF) in Prefrontal cortex (PFC) plays a key role both in learning-based spatial prioritization (Moore and Fallah 2001; Thompson and Bichot 2005; Squire et al. 2013; Gaspelin et al. 2015) and in the voluntary (Armstrong et al. 2009; Gregorious et al. 2009) and dynamic allocation of spatial attention (Astrand et al. 2016, 2018; Gaillard et al. 2020). Furthermore, neurons of this area are both involved in distractor suppression and target selection (Cosman et al. 2018), corroborating the idea of FEF as a critical neural node for the filtering visual information.

In the present study, we performed FEF neural recordings, while monkeys were engaged in a forced choice cued target detection task, in the presence of both task-relevant and task-irrelevant visual stimuli. Thanks to machine-learning methods applied to FEF activity, we decode the dynamic attention spotlight (AS) in order to explore the attentional filtering of the visual information with an unprecedented spatial and temporal resolution. In the following, we specifically describe distinct neuronal mechanisms associated with all of stimulus selection and suppression. We further provide behavioral and neural evidences demonstrating that 1) learning-based spatial prioritization is implemented independently from dynamic spatial attentional selection; 2) proactive and reactive suppression are implemented by two distinct neuro-cognitive mechanisms; and 3) reactive suppression is specific of irrelevant distractors and depends on the interplay of both learning-based and dynamic spatial prioritization mechanisms. Overall, we thus provide a unified neuronal framework of how the prefrontal cortex implements spatial selection and distractor suppression in order to flexibly optimize behavior in dynamic environments.

Materials and Methods

Subjects and Surgical Procedures

Two adult male rhesus monkeys (*Macaca mulatta*), weighing 8 kg (monkey D) and 7 kg (monkey HN), contributed to this experiment. Both monkeys underwent a unique surgery during which two MRI compatible recording chambers were implanted over the left and the right FEF hemispheres, respectively, as well as a head fixation post. Gas anesthesia was carried out using Vet-Flurane, following an induction with Zolétil 100. Post-surgery pain was controlled with a morphine pain-killer (Buprecare), three injections at 6-h interval (first injection at the beginning of the surgery) and a full antibiotic coverage was provided with Baytril 5%, one injection during the surgery and thereafter one each day during 10 days. A 0.6-mm isomorphic anatomical MRI scan was acquired post-surgically on a 1.5 T Siemens Sonata MRI scanner, while a high-contrast oil-filled 1 mm × 1 mm grid was placed in each recording chamber, in the same orientation as the final recording grid. This allowed a precise localization of the arcuate sulcus and surrounding gray matter underneath the recording chambers. The FEF was defined as the anterior bank of the arcuate sulcus and we specifically targeted those sites in which a significant visual and/or oculomotor activity was observed during a memory guided saccade task at 10°–15° of eccentricity from the fixation point. All surgical and experimental procedures were approved by the local animal care committee (C2EA42–13-02-0401-01) in compliance with the European Community Council, Directive 2010/63/UE on Animal Care.

Endogenous Cueing Detection Task and Experimental Setup

The task is a 100% validity endogenous cued luminance change detection task (Fig. 1A). The animals were placed in front of a PC monitor (1920 × 1200 pixels, refresh rate of 60 Hz) with their heads fixed. Stimulus presentation and behavioral responses were controlled using Presentation®. To start a trial, the monkeys had to hold a bar placed in front of their chair, thus interrupting an infrared beam. The appearance of a central fixation cross (size 0.7° × 0.7°) at the center of the screen, instructed the monkeys to maintain their eye position (Eye tracker—ISCAN, Inc.) inside a 2° × 2° window, throughout the duration of the trial, so as to avoid aborts. Four gray landmarks (size 0.5° × 0.5°) were displayed, simultaneously with the fixation cross, at the four corners of a hypothetical square having a diagonal length of ∼28° and a center coinciding with the fixation cross. The four landmarks (up-right, up-left, down-left, and down-right) were thus placed at the same distance from the center of the screen having an eccentricity of ∼14°. After a variable delay from fixation onset, ranging between 700 and 1200 ms, a 350-ms spatial cue (small green square—size 0.2° × 0.2°) was presented next to

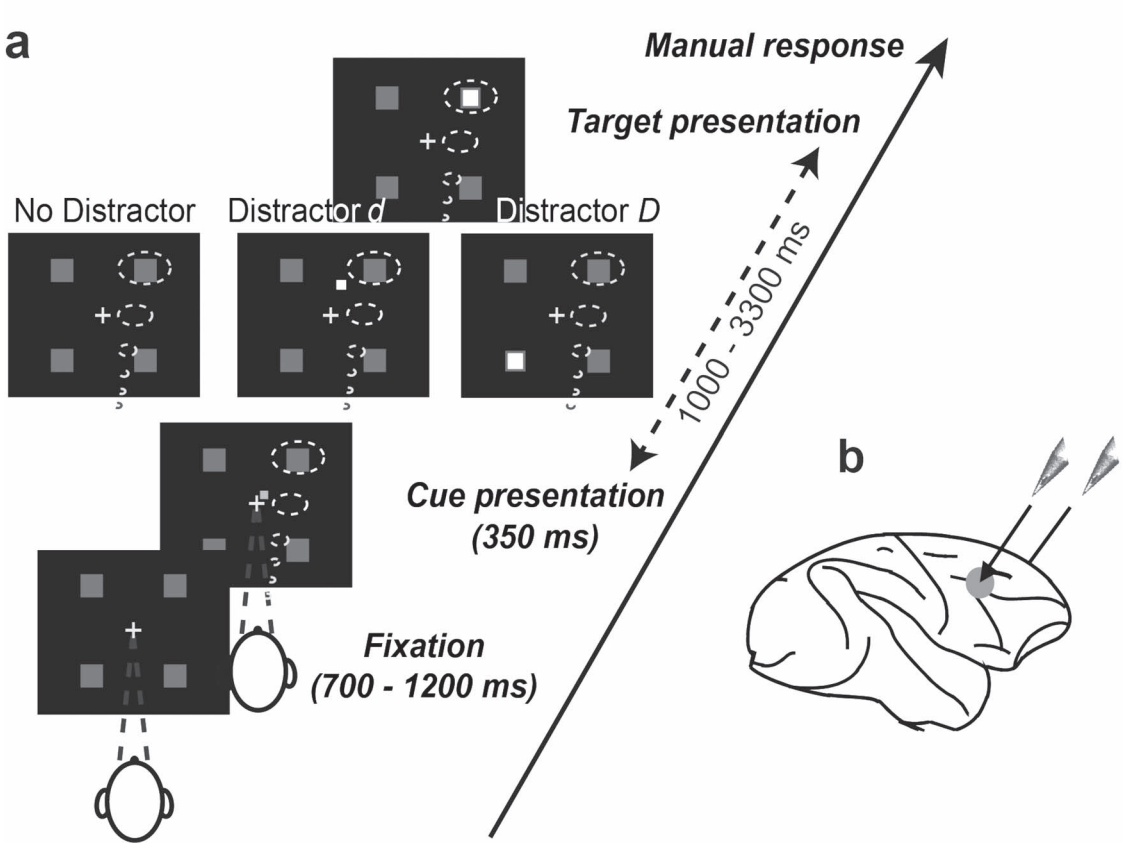

Figure 1. Task. (*A*) Behavioral task. Monkeys were required to produce a manual response to a cued target luminosity change while ignoring distractors presented at uncued landmarks (*D*) or elsewhere in the workspace (*d*). Central cross: fixation point. Green square: spatial cue. Dotted clouds: attention as cued by task instructions. (*B*) Recording sites. On each session, two 24-contact electrodes were placed in the right and left FEFs.

the fixation cross (at 0.3°), indicating the landmark in which the rewarding target change in luminosity would take place. Thus, the cue presentation instructed the monkeys to orient their attention toward the target in order to monitor it for a change in luminosity. The change in target luminosity occurred unpredictably between 1000 and 3300 ms from cue onset. In order to receive their reward (drop of juice), the monkeys were required to release the bar between 150 and 750 ms after target onset ("Hit"). To test the monkeys' ability at distractor filtering, on half of the trials, one of two distractor typologies was randomly presented during the cue-target delay, between 1000 and 3200 ms from cue onset. In ~17% of the trials (***D*** trials), a change in luminosity, identical to the awaited target luminosity change, took place at one of the three uncued landmarks. In these trials, the distractor *D* was thus identical in all respects to the expected target, except for being displayed in an uncued position. In ~33% trials (***d*** trials), a local change in luminosity (square) was displayed at a random position in the workspace. The size of the local change in luminosity was adjusted so as to account for the cortical magnification factor, growing from the center to the periphery (Schwartz 1994). In other words, *d* had the same size as *D* when presented at the same eccentricity as *D*. The absolute luminosity change with respect to the background was the same for both *d* and *D*. The monkeys had to ignore both the two distractor typologies (correct rejections—***RJ***). Responding to such distractors within 150–750 ms (false alarm—FA) or at any other irrelevant time in the task interrupted the trial. Failing to respond to the target ("Miss") similarly aborted the ongoing trial.

Electrophysiological Recordings and Spike Detection

Bilateral simultaneous recordings in the two FEF hemispheres were carried out using two 24-contact Plexon U-probes. The contacts had an interspacing distance of 250 μm. Neural data were acquired using a Plexon Omniplex® neuronal data acquisition system. The data were amplified 500 times and digitized at 40 000 Hz. Neuronal activity was high-pass filtered at 300 Hz and a threshold defining the multiunit activity (MUA) was applied independently for each recording contact and before the actual task-related recordings started. The LFPs were recorded simultaneously on the same electrodes as the spikes. LFP signals were digitized and sampled at 1 kHz and hardware filtered between 0.5 and 300 Hz, and a notch filter was applied online to remove any 50 Hz.

LFP and MUA Channels Selection

MUA and LFP signals used for all the analyses presented in this work were selected based on their target-related modulation. Specifically, MUA activity was smoothed using a 100-ms sliding window. For each of the four possible target locations, the mean (baseline) and the standard deviation (SD) preceding the corresponding target onset (time window [−200–0]) were calculated. A

channel was selected for the current analyses if the signal that followed target onset [20–400], overcame the baseline ±2.5∗SD for at least 100 ms and at least one target position. For LFP channels selection, we included only channels that were artifact- and noise-free in the voltage domain. We focused on LFP channels that contributed to target detection, that is, channels showing a different modulation when the animals correctly responded to the target (Hits) versus when they did not (Misses). We computed the SD of their baseline average difference, within each session, in the 200-ms epoch before target onset. To be selected, the voltage response of the considered channel had to cross a threshold of baseline average Hit-Miss difference ±2.5∗SD for at least 30 ms in the time window [30–230 ms] from target onset. Data analyses were performed using MATLAB (MathWorks).

Decoding Procedure

Training Procedure

Based on our prior work indicating that the endogenous orienting of attention can be reliably decoded from the FEFs using a regularized optimal linear estimator (RegOLE) (Farbod Kia et al. 2011; Astrand, Wardak, et al. 2014; Astrand et al. 2015, 2016), with the same accuracy as exogenous visual information, we trained a RegOLE to associate the neural responses (consisting in a vector containing the MUA signals collected at each of the 48 recording contacts) just prior to target onset ([−220 + 30] from target onset), for the first 200 correct trials, with the attended location, that is, with the expected target presentation landmark, based on cue information. Our general objective here was to have as precise as possible an estimate of the attention position before a specific visual event, averaging activities over large enough windows to have a reliable single trial estimate of the neuronal response on this window, while at the same time, a not too large time window to have a reliable estimate of where attention was placed by the subject at a specific time in the task (Farbod Kia et al. 2011; Gaillard and Hamed 2020). Differently from the neural analyses, the decoding procedure was performed including all the recorded channels within the session.

The RegOLE defines the weight matrix W that minimizes the mean square error of $C = W * (R + b)$, where C is the class (here, four possible spatial locations), b is the bias, and R is the neural response. To avoid over-fitting, we used a Tikhonov regularization (Astrand, Enel, et al. 2014; You et al. 2016) which gives us the following minimization equation: $\text{norm}\,(W*(R+b) - C) + \lambda*\text{norm}(W)$. The scaling factor λ was chosen to allow for a good compromise between learning and generalization. Specifically, the decoder was constructed using two independent regularized linear regressions, one classifying the x-axis (two possible classes: −1 or 1) and one classifying the y-axis (two possible classes: −1 or 1).

Testing Procedure

In order to identify the locus of attention at the moment of target or distractor presentation in the 20 next new trials following the initial training set, the weight matrix defined during training was applied to the average neuronal activity recorded in the 150 ms prior to either target or D and d distractors. The described training (over 200 previous trials)/testing (over 20 novel trials) procedure was repeated after every 20 correct responses, by retraining the decoder with the new database composed by the last 200 correct trials. This continuous updating of the weight matrix W is implemented in order to minimize the impact of possible uncontrolled for changes in the recorded signal during a given recording session onto the decoding procedure. Average decoding performance was 66,8% ± 2.6, in line with previous studies (Astrand et al. 2016), and significantly above chance, overall, as well as on individual recording sessions. The decoding of attention performed from the signal of the right Hemifield (54,44%) and from the signal left hemifield (54,99%) results comparable (Kruskal–Wallis nonparamteric test, $P = 0.94$). This is an indication that there were no biases in the hemifield representation in our data. Note that, expectedly, decoding performance using a unique probe is lower than the decoding performance using all 48 MUAs at once, due both to a better sampling of the entire visual field as well as to the use of more neuronal contacts.

(x,y) Spatial Locus of the Attentional Spotlight

As in Astrand et al. (2016), the readout of the RegOLE was not assigned to one of the four possible quadrants by applying a hardlim rule, as usually done for classification purposes. Rather, it was taken as reflecting the error of the decoder estimate to the target location, that is, in behavioral terms, as the actual (x,y) spatial estimate of the locus of the attentional focus to the expected target location. In Astrand et al. (2016) as well as in the present manuscript, we show that this (x,y) estimate of the AS accounts for variations in behavioral responses. In order to analyze how the distance of the decoded attentional spotlight to the target or to the distractor affected both behavior and neuronal MUA responses, we computed, for each target presentation and each distractor presentation, the distance between the decoded AS and the target (AT) or the distractor (AD or Ad) as follows: $AT = \sqrt{((x_{AS} - x_T)^2 + (y_{AS} - y_T)^2)}$, $AD = \sqrt{((x_{AS} - x_D)^2 + (y_{AS} - y_D)^2)}$, or $Ad = \sqrt{((x_{AS} - x_d)^2 + (y_{AS} - y_d)^2)}$, where x and y correspond to the Cartesian coordinates of the attentional spotlight, the target (T) or the distractors (D or d).

Statistical Assessment of Behavioral FA Rates

In order to statistically assess the dependence of FA rates onto the spatial position of d relative to both the target and attention, we estimated the 95% confidence interval limit using a one-tail nonparametric random permutation approach. For each d trial, we randomly reassigned its behavioral classification (i.e., Hit, FA, or Miss) and then we recalculated the FA rate (FAs/(Hits + FAs)). This procedure was repeated 1000 times and yielded a 1000 data points representing chance of FA rate distribution, and this for each spatial discretized position of d. FA rate for real nonpermuted data was considered significantly above chance if it fell within the 5% upper tail of its own spatial defined random permutation distribution.

Behavioral Responses Model Fitting Procedure

In order to determine the fitting model that best depicts the relationship between overt behavioral performance and the spatial position of the decoded attentional spotlight, we tested three regression models (linear, quadratic, and cubic) (cftool, Curve Fitting App. MATLAB®) and selected the one that provided the lower Akaike information criterion (AIC) (Choi and Kurozumi 2012), that is, minimizing $AIC = 2k + n\,\text{Log}(RSS/n)$, where k is the number of degrees of freedom used in the regression analysis, RSS is the residual sum of squares of the actual data to the fitting function, and n is the sample size. To avoid the risk of overfitting,

if two AIC values did not differ by more than 2 units, we chose the simplest model to explain the data.

Effect of Decoded Attentional Spotlight Location onto Target and Distractor-Related Neuronal Responses

In order to estimate the effect of the position of the decoded AS onto the neuronal responses to the target or to the distractor, for all trials in which the monkeys were cued to target *i* (*i* ranging from 1 to 4), instantaneous firing rates were normalized with respect to the peak average response to this target. Normalization was performed as follows: For each trial, raw firing rates were smoothed with a Gaussian kernel convolution procedure. Each of these smoothed firing rates was then normalized as follows: $Act_{i(Norm)} = (Act_i - Baseline_i)/(Peak_i - Baseline_i)$, where Act_i is the smoothed activity of the trial of interest in time (gaussian kernel, sigma = 25), in which attention is cued to target *i* (*i* ranging from 1 to 4), $Act_{i(Norm)}$ is this Act_i activity normalized in time, $Baseline_i$ is the average pre-target response to target *i* in the [−200–0] time interval with respect to target onset, and $Peak_i$ is the peak average response to target *i*. Trials were then categorized as a function of AT, AD, or Ad distance (see above). This normalization procedure thus allowed to quantify the influence of AT, AD, or Ad, irrespective of the neuron's attention or target related spatial selectivity.

Results

We recorded bilaterally from the FEFs of two macaque monkeys while they were required to perform a 100% validity endogenous cued luminance change detection task (Fig. 1A,B; monkeys' overall performance in the task is described in Supplementary note 1). In order to make sure that monkeys used the visual cues to orient their attention, two types of (to be ignored) distractors were also presented. Task-relevant distractors (*Ds*, ∼17% of the trials) were displayed in uncued target landmarks (landmarks), while task-irrelevant distractors (*ds*—the size of which was adapted so as to account for the cortical magnification factor (Carrasco and Frieder 1997), ∼33% of the trials) were presented randomly in the visual workspace. These two types of distractors shared the same shape and same relative visual contrast. They only differed in where they could be expected to be presented: either at task relevant landmark or at task-irrelevant locations. These distractors were exclusively presented during the attention-orientation epoch, that is, to say between cue and target presentation, as illustrated in Figure 1A. Supplementary Figure 1 and Supplementary note 2 describe the attention orientation and target detection neuronal response properties in the recorded signals. Importantly, and in contrast with previous studies, behavioral and neuronal responses are analyzed either 1) as a function of the physical configuration of the task, thus defining the task-based spatial priority map, or 2) as a function of the time-resolved readout of the position of the AS from the FEF population activity, just prior to stimulus presentation, thus defining the dynamic spatial filtering of visual information by the AS. This approach is based on machine-learning decoding procedures applied to the PFC activity (Astrand et al. 2016; Gaillard et al. 2020), and allows to estimate the position of the AS in the visual workspace. Its outcome has been shown to be highly predictive of overt behavioral performance and reaction times (Astrand et al. 2016, 2020, Gaillard et al. 2020, Sousa et al. 2021), thus indicating that it reliably reflects the underlying function (Supplementary note 3).

Behavioral and Neuronal Correlates of the Task-Based Spatial Priority Map

The processing of stimuli located in the vicinity of the expected target location is enhanced (Bettencourt and Somers 2009; Suzuki and Gottlieb 2013). This is thought to result from top-down contingent selection mechanisms (Noudoost et al. 2010; Ibos et al. 2013; Chica et al. 2014). However, by virtue of trial configuration, repetition, and learning, uncued target placeholders are also prioritized with respect to the background; this irrespective of current trial cueing information (Chelazzi et al. 2013; Jiang et al. 2018). Spatial prioritization is probed by measuring FA rates produced by distractors presented in the vicinity of the key items of the task. Importantly, these distractors were adjusted in size depending on what eccentricity they were presented at, thus compensating for cortical magnification. Accordingly, FA rates and neuronal responses to these distractors did not vary between central and more eccentric distractors (Supplementary Fig. 2, FA rates: Kruskal–Wallis nonparametric test, $P = 0.57$; neuronal responses: Kruskal–Wallis nonparametric test, $P = 0.39$). In this first section, we characterize the behavioral and prefrontal neuronal signatures of task-based spatial prioritization, at both the cued and uncued landmarks. We measure FA rates to *d* distractors, presented randomly throughout the visual workspace. For data analysis, on each trial, we flip the visual space such that target location coincides with the upper right visual quadrant, and the uncued quadrant ipsilateral to the target falls in the lower right visual quadrant. We compute FA rates at a $3° \times 3°$ spatial resolution, cumulating behavioral data over all trials and all sessions (Fig. 2A). Expectedly, FAs are significantly enhanced around the cued target location (Fig. 2A, top right quadrant, ∗, beyond the 95% confidence interval defined by a one-tail random permutation test). FAs are also significantly enhanced around the uncued landmarks (Fig. 2A, top left and bottom left and right quadrants). Visual space in the vicinity of the uncued landmarks (Fig. 2B—left panel; light gray area, FA rate = 14,0%) shows higher FA rates compared with areas with equivalent T*d* distance (6,92%, dark gray area, Kruskal–Wallis nonparamteric test, $P < 0.05$) or shorter (7,14%, brown area, Kruskal–Wallis nonparamteric test, $P < 0.05$) but located away from these locations. In other words, both the cued and the uncued landmarks are prioritized on any given trial. This is in agreement with the demonstration that rewarded spatial contingencies exert a powerful influence on the attentional control deployment (Della Libera and Chelazzi 2009; Chelazzi et al. 2013), such that uncued target location might assume a high behavioral relevance including when not currently used as a target. Due to cue benefit, on any single trial, the cued landmark is more prioritized than the other landmarks (see next section).

FA rates drastically decrease as the distance between distractors and expected target location increases (Fig. 2B); all sessions cumulated and binned as a function of T*d*—from 0° to 22°, step 0.5°, reproducing previous observations, for example, Suzuki and Gottlieb (2013). This relationship is best fit by a third-order polynomial function characterized by a steep initial decrease in FAs away from the target and a small rebound for T*d* beyond 14° (see Methods, r^2 adjusted = 0.972, AIC = 1068.9). This rebound is probably driven by the observed spatial prioritization around

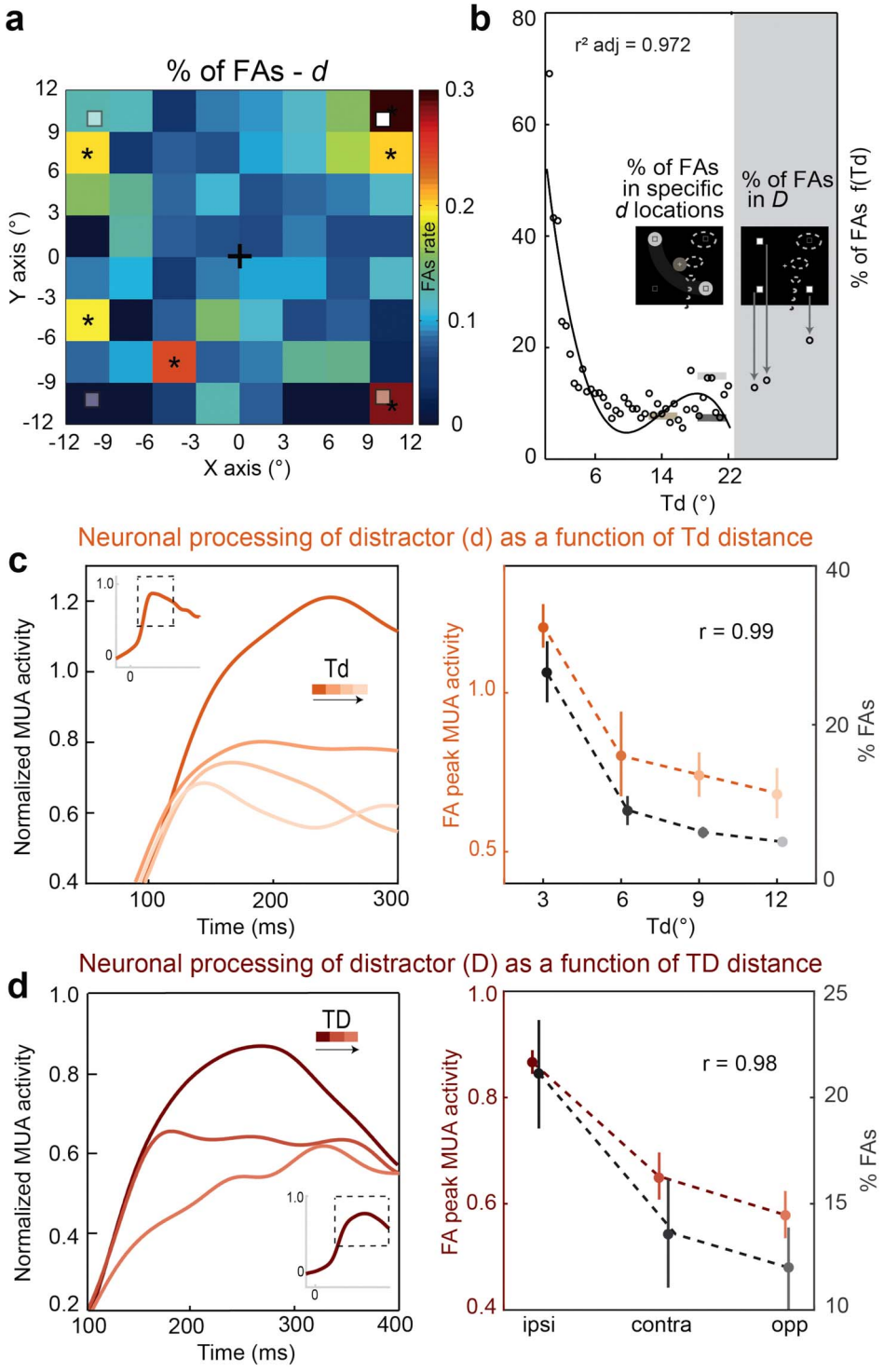

Figure 2. Behavioral and neuronal spatial priority map. (*A*) Spatial map of FA rates as a function of the location of distractor (*d*) in the workspace. In order to cumulate behavioral responses over trials of different spatial configurations, trials are flipped such that target location coincides with the upper right visual quadrant, and the ipsilateral uncued quadrant falls in the lower right visual quadrant. FA rates (%, color scale) are computed independently for distractors (*d*) presented in (3° × 3°) adjacent portions of the workspace. Black asterisks indicate FA rates significantly higher than chance, as estimated by a one-tail random permutation test (<95% confidence interval). (*B*) FA rates as a function of the distance between the target and distractor *d* (Td, left) or distractor *D* (TD, right). Black line corresponds to the third-order polynomial regression best fit. Horizontal colored lines indicate the FA rate for trials in which *d* happened in specific areas of the visual scene as shown in the inner panel left (light gray, around the ipsilateral or the contralateral landmark [LM*d* = 0° ± 2°]; dark gray: at T*d* = 20° ± 2°, excluding distractors *d* close to landmarks [±2°]; light brown: around the fixation cross [F*d* = 0° ± 2°]). Right panel: FA rates elicited by distractors *D*, for each of the three possible locations. (*C*) Neural FA responses as a function of the distance between distractor *d* and Target (T*d*), and associated performance. Left panel: Normalized neural response to *d* as a function of T*d*. Four ranges of T*d* were considered for the trials' selection from 0° (dark orange) to 12° (light orange) in T*d* steps of 3° (intermediate shades of orange). The inset panel represents

the ipsilateral and contralateral uncued LMs (Fig. 2B, left panel, light gray shaded bar).

Similar to the behavioral prioritization of task relevant locations, the evoked visual neuronal response to *d* on FA trials strongly depends on T*d* (Fig. 2C, left panel, note only target modulated MUAs are included in the analysis, see Supplementary note 4 for a description of trial number per T*d*), reproducing prior observations (e.g., Suzuki and Gottlieb 2013). The same trend is reproduced for correct rejection trials, although to a lesser extent due to distractor suppression (see Supplementary Figure 3 and next sections). In addition, this observation is also reproduced whether considering only *d* distractors falling in the preferred quadrant (i.e., within the visual receptive field) or in the antipreferred quadrant (i.e., in the surround of the visual receptive fields, Supplementary Fig. 4, left panels). Last, this is also reproduced for *D* distractors (Supplementary Fig. 4, right panels). This neuronal tuning curve as a function of T*d* follows the same shape and is highly correlated to the FA rate as a function of T*d* ($r = 0.99$, $P < 0.001$, Fig. 2C, right panel), suggesting a tight functional link between these two measures. Likewise, the evoked visual neuronal response to *D* distractor on FA trials strongly depends on TD (Fig. 2D, left panel, note though that for equal TD, neuronal response to ipsilateral *D* is higher than for contralateral *D*). Similarly, the neuronal tuning curve and the FA rate as a function of TD are correlated with each other ($r = 0.98$, $P < 0.05$, Fig. 2D, right panel). Overall, we thus show that FEF neuronal responses to visual stimuli of equalized contrast and visual energy are modulated by task-related contingencies in close correspondence with the behavioral characterization of the spatial priority map.

The Attentional Spotlight Dynamically Implements Target Selection Independently of the Spatial Priority Map

Spatial attention is hypothesized to act as a spatial filtering "in" mechanism, which enhances the selection of incoming visual stimuli depending on their distance to its focus (Theeuwes 2010; Chelazzi et al. 2019; Hembrook-Short et al. 2019). This attention-based spatial filtering is often equated with spatial prioritization by cue instruction. However, recent studies demonstrate that spatial attention is not stable and samples space rhythmically including following a spatial cue (Landau and Fries 2012; Fiebelkorn et al. 2013; Spyropoulos et al. 2018; Gaillard and Hamed 2020). In the following, we demonstrate the existence of a dynamic prioritization of space by the attentional spotlight, independent of the task driven trial prioritization by cue instruction described in the previous section. To this effect, we use machine learning to access the time-resolved readout of the (*x*,*y*) position of the AS from the FEF population activity prior to target presentation (Astrand et al. 2016; Gaillard et al. 2020). As expected from task instructions, AS is mostly allocated within the cued quadrant, but not necessarily at the exact target location (Supplementary Fig. 5). We analyze normalized FEF neuronal responses to target presentation as a function of the distance of the AS to the target.

Figure 3A shows the average normalized neuronal responses to the target (target selective MUA channels, normalized activities, $n = 562$, see Materials and Methods), on Hits (blue) and Misses (yellow). On Hit trials, a marked response to target presentation is observed, peaking at 285 ms following stimulus onset (Fig. 3A, blue curve). On Miss trials, the neuronal response was significantly weaker (Fig. 3A, yellow curve, Kruskal–Wallis nonparametric test, $P < 0.001$). This confirms the well-known critical contribution of FEF to sensory selection for perception (Thompson et al. 1997; Thompson 2005; van Vugt et al. 2018). Importantly, we show a direct modulation of both the behavior and the evoked neuronal response to target processing by the position of the AS. Specifically, we categorize neuronal responses (Fig. 3B, all sessions cumulated and binned as a function of AT, from 0° to 24°—step 4°, Fig. 3C, blue curve and scale) as well as behavioral performance (Fig. 3C, black curve and scale) as a function of the distance between the AS and the target (AT). The strength of the neuronal response to detected targets decreases as AT increases (Fig. 3B,C, blue curve, Kruskal–Wallis nonparametric test, $P < 0.001$). Likewise, the behavioral performance constantly decreased as AT increased (Fig. 3C, black curve, Kruskal–Wallis nonparametric test, $P < 0.001$). The effect of AT onto neuronal peak responses to detected targets and behavioral performance was highly correlated (Fig. 3C, $r = 0.85$, $P = 0.03$), both showing significantly higher values when the AS was close to the target. Overall, this is, to our knowledge, the first direct neurophysiological evidence for an attentional spatial filtering "in" or attention selection neuronal function centered onto the AS (Downing and Pinker 1985). Most importantly, this AS spatial filter is independent from the spatial priority map described above and can only be accessed through a direct estimate of covert AS at an appropriate temporal resolution.

The Attentional Spotlight Dynamically Implements Both the Selection of Task Relevant Items and the Suppression of Task Irrelevant Items

A major question in the field is whether distractor suppression is implemented by the same neuronal mechanisms as target selection, whereby vicinity of the AS to the incoming sensory stimulus defines the degree of selection/suppression that is applied (Suzuki and Gottlieb 2013; Cosman et al. 2018). In the following, we demonstrate that the prefrontal AS can both select (filter "in") or suppress (filter "out") incoming sensory information depending on task configuration. Specifically, we analyze the behavioral performance and the FEF neuronal response on FA responses to *D* (task-relevant distractors) or *d* (task-irrelevant distractors), as a function of their distance to AS location in space just prior to their presentation (resp. A*D* and A*d*, Fig. 4, all sessions cumulated and binned as a function of A*D* and A*d*, respectively). The closer the AS to *D*, the higher the probability of FAs (Fig. 4A, right panel, gray curve, Kruskal–Wallis nonparametric test, $P < 0.001$, see Supplementary note 4 for a description

the averaged neuronal response to FAs when $0° < Td < 12°$. Right panel: Demeaned peak neuronal responses (orange) and behavioral performance (black), as a function of T*d*. T*d* categories and colors as in left panel. Error bars represent mean ± SE. (*D*) Neural FA responses as a function of D position, and associated performance. Left panel: Normalized neural response to *D* as a function of TD, for the ipsilateral (dark red, ipsi), the contralateral (medium red, contra), and the opposite landmark (light red, opp). Right panel: Demeaned peak neuronal responses (red) and behavioral performance (black), as a function of TD. TD categories and colors as in left panel. Error bars represent mean ± SE.

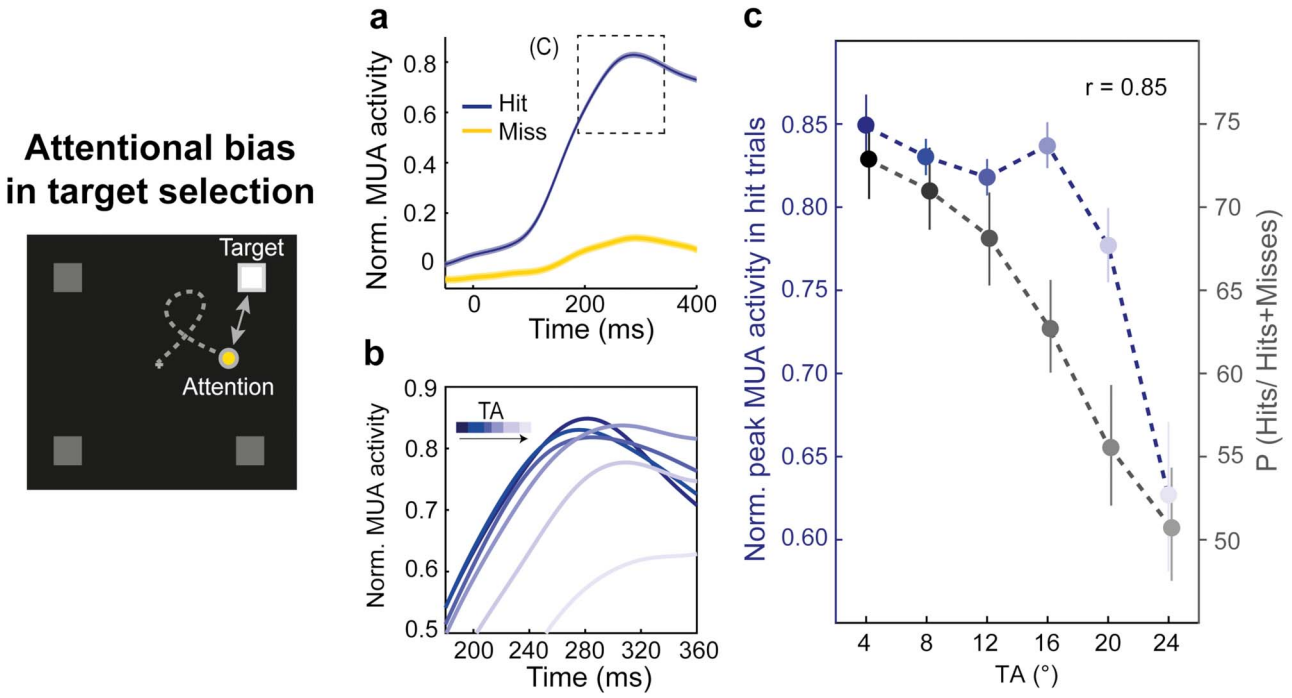

Figure 3. Neural responses to the target as a function of the distance between the target and the decoded attentional spotlight (TA). (*A*) Normalized MUA population response to the target, on Hits (blue) and Misses (yellow). Shaded error bars represent ± SE. (*B*) Normalized neural responsiveness to the target, on Hit trials, as a function of TA (inset in panel A). Six ranges of TA were considered for the trials' categorization from 0° (dark blue) to 24° (light blue) in TA steps of 4° (intermediate shades of blue). (*C*) Demeaned peak responses and behavioral performance as a function of TA. TA categories and colors as in panel *B*. Error bars represent ± SE.

of trial number per A*D*). The same observation is reproduced for individual cue instructions (Supplementary Fig. 7). This relationship is best modeled by a linear fit (Supplementary Fig. 6*a*, r^2 adjusted = 0.85, $P < 0.001$, best-fit achieved by the linear model, AIC = 41.65), reproducing our previous observations on a different dataset (Astrand et al. 2016). Mirroring the relationship between behavioral performance and A*D*, the neuronal response to *D* also increases as A*D* decreases (Fig. 4A, middle panel, dark–light red curves, Kruskal–Wallis nonparametric test, $P < 0.001$). The relationship between average peak neuronal response to *D* and A*D* on the one hand, and FA rates and A*D* on the other hand show a trend toward correlation (Fig. 4A, $r = 0.92$, $P = 0.08$). These observations are remarkably similar to those reported for target selection whereby visual information close to the AS is filtered "in," while visual information far away from the AS is suppressed and filtered "out."

D distractors are, by definition, presented in a prioritized position of the spatial priority map (uncued target landmarks—Fig. 2C). An important question is thus whether the spatial prioritization filtering "in" process described above for *D* distractors also generalizes to *d* distractor presented at irrelevant locations. These *d* distractors could unpredictably appear anywhere onto the visual scene, they had the same shape and the same contrast as *D* distractors, and their size was adjusted to compensate for the cortical magnification factor (see Materials and Methods). Trials were sorted as a function of the distance between the AS and *d* distractors (Fig. 4B—lower panel, all sessions cumulated and binned as a function of A*d*—from 0° to 12°, step 3°, see Supplementary note 4 for a description of trial number per A*d*). To avoid possible confounds due to the heterogeneity of the spatial priority map, this analysis is restricted to *d* distractors presented in the cued quadrant. In this range, the distribution of A*d* did not differ for different TA categories (Supplementary Fig. 8, A*d* in TA ranges of 5°, Kruskal–Wallis, $P = 0.10$). In contrast with the *D* prioritization process described above, we found that the closer the AS to *d*, the lower the FA probability, indicating that the AS suppresses *d* distractors rather than enhances them. The attentional profile that characterizes this *d* suppression is not linear. Rather, best fit is achieved by a third-order polynomial model (Supplementary Fig. 6*b*, r^2 adjusted = 0.18, AIC = 47.94). Specifically, FA rates were marginally lower when $Ad < 3°$ than when $3° < Ad < 6°$ (Supplementary Fig. 1c, black curve, all sessions cumulated and binned as a function of A*d*—from 0° to 12°, step 3°, post-hoc Friedman rank sum test, $P = 0.097$) and significantly lower than when $6° < Ad < 9°$ (post-hoc Friedman rank sum test, $P < 0.01$). Beyond A*d* of 9°, FA rates dropped instead of increasing (post-hoc Friedman rank sum test, $P < 0.05$), thus roughly defining an inverted Mexican hat shaped function. This filtering profile was drastically different from the one reported for *D*. Importantly, this filtering profile did not result from an interaction with the spatial priority map and T*d*. Indeed, the same statistical trends emerged both when *d* distractors were close ($Td < 7°$) or far ($7° < Td < 14°$) from the target (Supplementary Fig. 1c, gray curves—Kruskal–Wallis, main A*d* distance effect, $P < 0.05$). The relationship of the neuronal response with A*d* mirrored that of the behavioral performance (Fig. 4B, middle panel, dark–light red curves, Kruskal–Wallis nonparametric test, $P < 0.001$). Peak neuronal responses to *d* distractors for $Ad < 3°$ trials were significantly lower than for $3° < Ad < 6°$ and for $6° < Ad < 9°$, but higher than those within $9° < Ad < 12°$ (post-hoc Friedman rank sum test; $P < 0.05$, $P < 0.001$, $P < 0.001$, resp.). The relationship between average peak neuronal response to *d* and A*d* on the one

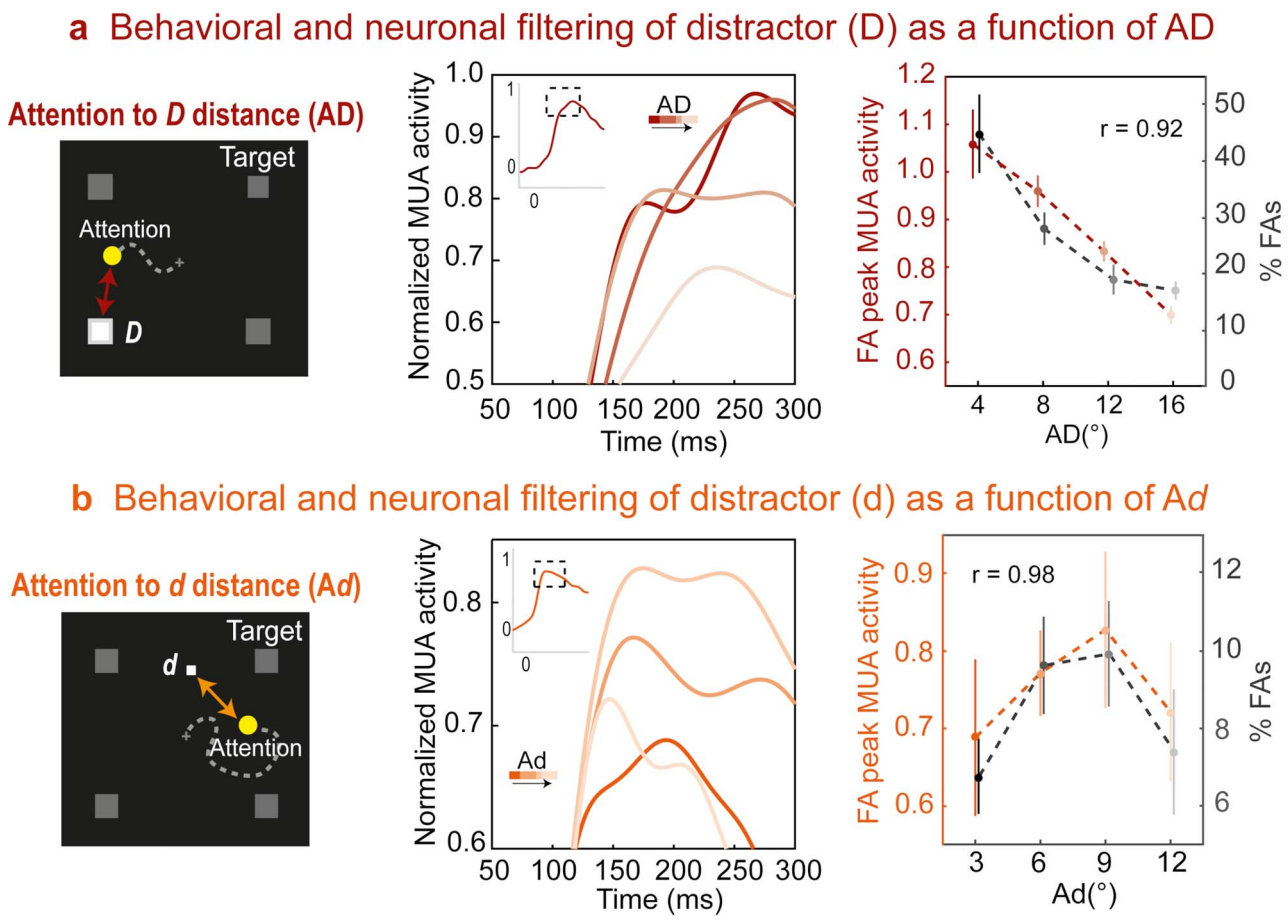

Figure 4. Neural responses to distractor as a function of the distance between *D* distractors and the decoded attentional spotlight (AD, panel *A*) and *d* distractors and the decoded attentional spotlight (Ad, panel *B*), on FA trials. *AD* distances (intermediate shades of red) ranged from 0° to 16° (step = 4°). *Ad* distances (intermediate shades of orange) ranged from 0° to 12° (step = 3°). All else as in Figure 3.

hand, and FA rates and A*d* on the other hand were highly correlated (Fig. 4*B*, right panel, $r = 0.98$, $P < 0.02$). This observation is evidence for an inversed center-surround functional filtering profile by the AS. Such a function can also be viewed as a suppression mechanism implemented by a classical Mexican hat AS. This difference in the response to *D* and *d* distractors cannot be accounted for by the physical presence of the landmarks (Supplementary note 5). It is noteworthy at this stage that distractor presentation, for both types of distractors, triggers a re-orienting or attention away from its initial position (see Supplementary note 6), confirming our previous observations in a different dataset (Astrand et al. 2020).

Overall, we thus describe two distinct filtering mechanisms implemented by the dynamic AS: a prioritizing, filtering "in" process and a suppressive, filtering "out" process. The implementation of one or the other does not depend on the prioritization map but rather on the sensory item's task relevance.

Neural Evidence for Distinct Proactive and Reactive Suppression Mechanisms

The above described distractor selection and suppression mechanisms coincide with major differences in neuronal responses to correctly rejected (RJ) distractors. Figure 5A reports averaged normalized neuronal responses (target selective MUA channels, D = 340, HN = 222) on FA (red shades) and correct rejection trials (green shades), for *D* (left panel) and *d* distractor (right panel). Overall FAs showed a marked neuronal response for both *D* (Fig. 5A, left panel, *D*FAs, 0.78 ± 0.12, peak latency = 267 ms) and *d* distractors (right panel, *d*FAs, normalized peak response, 0.80 ± 0.04, latency = 165 ms, note that on these trials, neuronal predistractor response is higher for FAs than for correct rejections due to the fact that FAs are more frequent for *d* distractors close to the cued landmark). These responses are very similar to those observed to targets on Hit trials (Fig. 3A, 0.83 ± 0.006) and they coincide with a marked visual evoked potential in the LFPs (Fig. 5B, left panel, *D*FA and Hits, right panel, *d*FA). In contrast, neuronal responses on correct rejection trials show very distinct patterns for the two types of distractors (Fig. 5A,*B*). Correct rejection to *D* distractors barely responds to distractor presentation (Fig. 5A, left panel, *D*RJs, 0.09 ± 0.06), while correct rejection to *d* distractors exhibits a clear phasic response (Fig. 5A, right panel, *d*RJs, 0.3 ± 0.01, peak latency = 147 ms). The average normalized MUA net response estimated as the difference between peak and predistractor baseline (Fig. 5C), showed enhanced responses on FA trials as compared with correct rejections to both *D* and *d* distractors (Kruskal–Wallis nonparametric test, $P < 0.001$). However, while there was no difference between *d*FA (0.72 ± 0.08) and *D*FA trials (0.83 ± 0.09, Kruskal–Wallis nonparametric test, $P = 0.32$), this difference was significantly higher on *d*RJs trials

(0.56 ± 0.02) than on DRJs trials (0.23 ± 0.06, Kruskal–Wallis nonparametric test, $P < 0.001$). This coincides with a very small LFP visual evoked potential for DRJ (Fig. 5B, left panel) and a marked LFP visual evoked potential for dRJ (Fig. 5B, right panel). This strongly suggests that dRJ takes place subsequently to perception. Indeed, while MUA results from local neural processing, informing on how the sensory representations in dendritic input are transformed into cognitive signals, LFP provides a measure of both the local processing and synaptic inputs from other brain regions (Nielsen et al. 2006; Monosov et al. 2008; Gregoriou et al. 2009; Einevoll et al. 2013).

In other words, the successful suppression of D is thus accompanied by a proactive suppression of the visual input to the FEF. In contrast, the successful suppression of d is accompanied by a strong visual input to the FEF, indicating that suppression takes place following sensory processing and perception. This indicates the existence of two distinct suppression mechanisms: a proactive suppression mechanism associated with D, and a reactive suppression mechanism associated with d.

Several studies support the idea that reactive suppression is implemented in the prefrontal cortex and specifically in the FEF (Hasegawa et al. 2004; Marini et al. 2016; Cosman et al. 2018). Further supporting this point, we show here that the peak neuronal response to d distractors on dRJ trials is rapidly followed by a sharp decrease in the neuronal response (Fig. 5D, left panel, arrow, Ranksum test, $P < 0.001$) that brings the neuronal response down to the same level as in DRJ trials. This effect is hardly present on these DRJ trials (Fig. 5D, right panel) and is absent in FA trials as well as in Hit trials. This active suppression mechanism takes place right after peak distractor response (at an average timing of 147 ms), which is compatible with an interruption of the motor response (median RT = 447 ms). The latency of the suppressive dip from the d distractor peak response is of 322 ms. This timing coincides with the estimated time needed to overtly reject low saliency distractors as task irrelevant (150–300 ms—Geng 2014). While this timing is compatible with a polysynaptic transmission, reactive suppression is expected to be based on a perceptual decision that is known to take place in the prefrontal cortex (Ibos et al. 2013; van Vugt et al. 2018). In the following, we explore the functional relationship between enhanced perception by the AS and reactive suppression.

The Attentional Spotlight Dynamically Implements Reactive Suppression

Our work indicates that reactive suppression is associated with two distinct components: 1) a strong visual evoked response to the distractor and 2) a subsequent strong suppression discriminating between correct rejections and FAs. A key question is thus to characterize whether suppression depends on prior perception. In the first two sections of this paper, we describe two main factors that influence how stimuli of the same visual salience are perceived: 1) the spatial priority map defined by Td and 2) the dynamic attentional selection defined by Ad. In the following, we further quantify the impact of these two task-related factors onto the degree to which the initial perceptual response is suppressed following a d distractor presentation.

Figure 6 shows the average normalized MUA response to Td (Fig. 6A, left panel) and Ad (Fig. 6B, left panel, specifically for $Td < 3°$), irrespective of predistractor response level. This allows

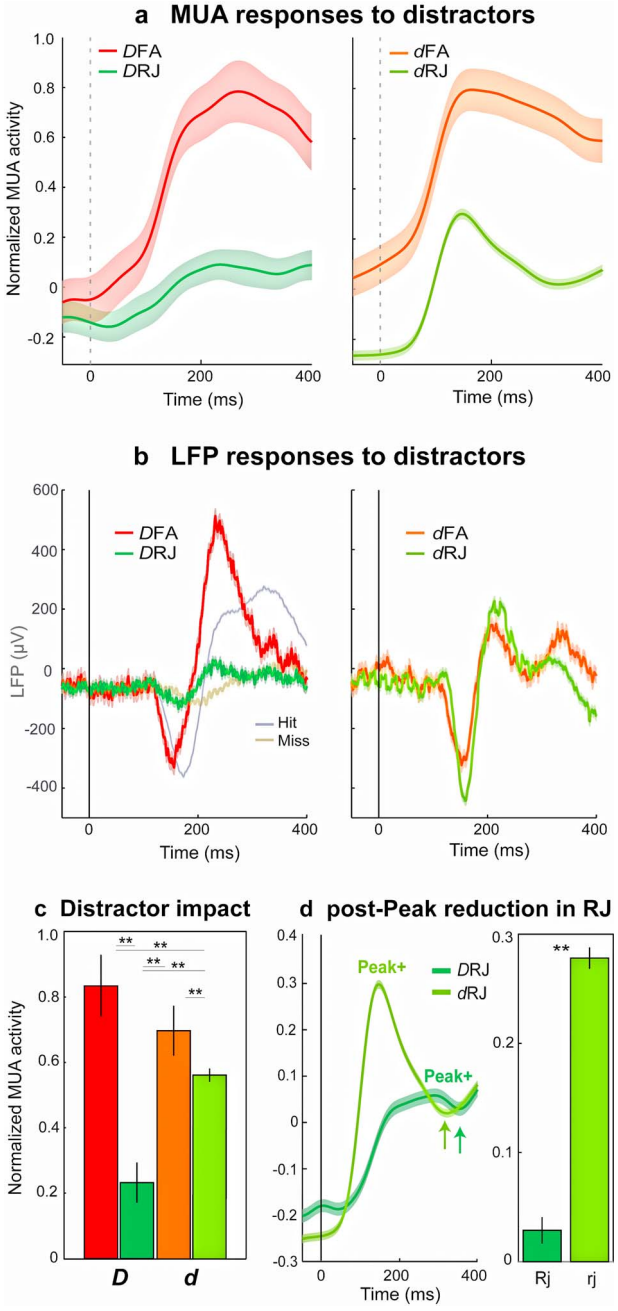

Figure 5. Neural correlates of proactive and reactive distractor suppression. (A) Normalized MUA population responses to D, in DFAs (FAs, dark red) and DRJs (correct rejections, dark green), and to d, for dFAs (orange) and dRJs (light green). Left panel: Average normalized MUA, around distractor D onset for DFAs (dark red) and DRJs (dark green). Right panel: Average normalized MUA, around distractor d onset, for dFAs and dRJs. Shaded error bars, ±1 SE. (B) LFP modulation as a function of trial types. Left panel: Average LFPs, around target onset for Hits (blue) and Misses (yellow) and around distractor D onset for DFAs (dark red) and DRJs (dark green). Right panel: Average LFPs around distractor d onset, for dFAs and dRJs. Shaded error bars, ±1 SE. (C) Difference between peak response to distractor and predistractor baseline, in DFAs (dark red) and DRJs (dark green), and to d, in dFAs (orange) and dRJs (light green). Error bars, ±1 SE. (D) Neural responses to DRJ and dRJ. Left panel: "Peak+" indicates, for each signal, peak response in the [0350 ms] time interval following target onset. Arrows indicate, for each signal, the average time of the first signal dip following the identified peak. Right panel: neural suppression measured as the difference between identified peaks and dips (mean ± SE), for D (dark green) and d (light green) trials. Asterisks indicate statistical significance as assessed by a Wilkoxon rank sum test (**$P < 0.001$).

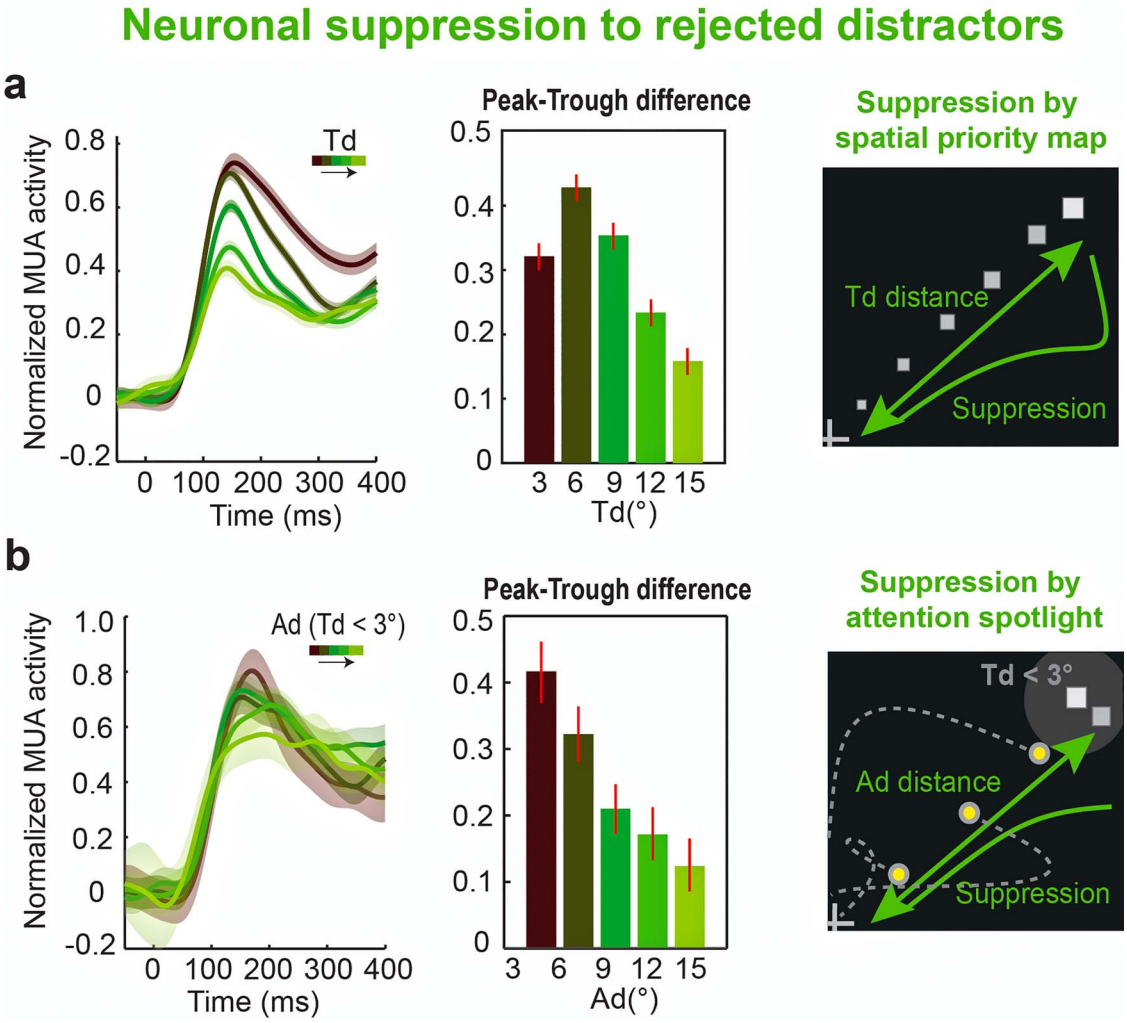

Figure 6. Neural reactiveness in distractor *d* correct rejection trials as a function of the distance between distractor (*d*) and the Target (T*d*, panel *A*) and distractor (*d*) and the decoded attentional spotlight (A*d*, panel *B*). Both T*d* and A*d* distances are represented in shades of green and ranged from 0° to 15° (step = 3°). Middle panels represent the normalized MUA difference in activity between the peak and trough of distractor related responses on correct rejection trials.

to specifically estimate the impact of *d* onto FEF neural processing. While for T*d* eccentricity beyond 3°, postevoked response suppression decreased as T*d* increased, all evoked responses being suppressed down to the same level; suppression was significantly reduced for shorter T*d* distances (T*d* < 3°, Fig. 6*A*, middle panel, Kruskal–Wallis, $P < 0.01$).

Hypothesizing that for shortest T*d* distances, accurate perception is critical to disambiguate between a target and a distractor, we focused on these specific trials, and we quantified how A*d* distance impacted the overall level of suppression of the evoked response. This analysis is presented in Figure 6*B*. As seen previously for FAs (see also Supplementary Fig. 9), on correct rejections, the visual evoked response to distractor presentation was strongest for short A*d* than for longer A*d* (Fig. 6*B*, left panel). Importantly, suppression strength was also highest for short A*d* than for longer A*d* (Fig. 6*B*, middle panel, Kruskal–Wallis, $P < 0.05$). In FA trials, in which attention suppression was less effective, the strength of this neuronal suppression is less marked, though still highest for shorter A*d* distances than for intermediate A*d* distances (Supplementary Fig. 9, Kruskal–Wallis, $P < 0.05$). Overall, this indicates that both spatial prioritization by the spatial priority map and the dynamic attentional spotlight contribute to influence perception, stimulus selection, and stimulus suppression.

Discussion

Overall, we thus identify, in the FEF, distinct neuronal mechanisms, respectively, implementing proactive and reactive suppression mechanisms (Chelazzi et al. 2019). We further show that the implementation of both these suppressive mechanisms depends on the learned task-based priority map (Chelazzi et al. 2014; Awh et al. 2012; Moore and Zirnsak 2017; Ferrante et al. 2018) as well as on the dynamic spatial filtering implemented by the attentional spotlight as it dynamically and rhythmically explores the visual scene. While the spatial priority map exclusively defines a spatial filtering "in" function, the dynamic attentional spotlight defines both a spatial filtering "in" and a spatial filtering "out" function. The top-down attention-based spatial filtering "in" is associated with the proactive suppression of task relevant distractors, while the attention-based spatial filtering "out" is associated with the reactive

suppression of task irrelevant distractors. This is further discussed below.

Multiple Mechanisms of Spatial Visual Selection

Sensory selection of visual input can be dynamically deployed at will by spatial attention (spatial orienting of attention, Astrand et al. 2016; Gaillard et al. 2020) or can result from the learning of task contingencies (a task-based priority map, Awh et al. 2012; Anderson and Britton 2020). Here, we provide behavioral and neural evidence indicating that both attentional mechanisms independently contribute to stimulus selection.

Task-Based Priority Map

The filtering of irrelevant visual information is not uniform across the visual scene. Rather, distractibility, that is to say, inappropriate responses to irrelevant visual stimuli, is maximal in the vicinity of the four spatial locations at which the target can be presented on each trial, by task design. This spatial prioritization reflects the learning of the experienced rewarded-stimuli contingencies characterizing the task (Chelazzi et al. 2013). Our observations indicate that the FEF implements a task-based spatial priority map, showing enhanced neural responses to stimuli that are closest to the prioritized spatial locations as compared with the rest of the visual scene. This prioritization roughly follows a Gaussian filtering function and almost disappears beyond 6° away from the prioritized location. This neuronal filtering function strongly correlates with behavioral distractor interference measures, suggesting a strong functional relationship between FEF prioritization map and overt behavior.

An important question is whether this learned task-based spatial prioritization arises from a top down control mechanism or from long-lasting changes in the excitability of the topographically organized spatial maps. Such changes in local neuronal excitability through statistical learning and cumulative experience have already been demonstrated in the primary visual cortex (McManus et al. 2011; Gilbert and Li 2013). Whether this also takes place at higher levels of the visual hierarchy, for example, in the parietal or in the prefrontal salience maps is unclear. In our hands, the selection of irrelevant visual items is weaker close to prioritized locations that are contralateral to the cued target location as compared with prioritized locations that are ipsilateral to the cued target location. This thus indicates an interaction between top-down spatial cueing information and task-based prioritization, whereby although experience with the task based contingencies has induced long lasting changes in the FEF spatial priority map, these changes are potentiated by cueing instructions on each given trial. Importantly, this interaction is independent of the dynamic spatial orienting of attention during the cue to target interval.

Spatial Attention Orienting

Classically, attention orientation is confounded with cuing information. Thanks to a spatially and temporally resolved decoding of the locus of the attentional spotlight, we have already shown that this attentional spotlight is highly dynamic and not constrained to the cued location (Astrand et al. 2016; Gaillard et al. 2020). Here, we show that the perception of a low saliency stimulus depends on the position of the attentional spotlight just prior to stimulus presentation. We provide the first direct estimate of the spatial attention filtering function hypothesized as early as the seminal work of James (1890). Importantly, and in contrast with the classical view of attention spatial filtering, we identify two distinct spatial attention filtering functions. 1) The closer the attentional spotlight to task relevant stimuli, the higher report probability, our proxy for visual perception. This corresponds to a filtering "in" attentional function, whereby sensory information is selected when presented at the center of the dynamic attentional spotlight, while the probability of visual selection decreases along a coarsely Gaussian shaped function as the sensory information is presented further and further away from the center of the attentional spotlight. This filtering function applies both to targets presented at the cued location and to relevant (target-like) distractors presented at uncued locations prioritized by the statistical learning described above. 2) In contrast, the closer the attentional spotlight to task irrelevant stimuli, the lower report probability. This thus corresponds to a filtering "out" attentional function, whereby sensory information is suppressed when presented at the center of the dynamic attentional spotlight. This filtering "out" attentional function is characterized by an inverted "Mexican hat" shape, defining a suppressive center around the attentional spotlight, a first surround in which this suppressive filter weakens and a final surround in which suppression increases again, probably by sheer distance from the center of the attentional spotlight, the stimulus falling outside the perceptual spatial extent of the attentional spotlight. Overall, spatial attention thus implements a dynamic spatial perceptual gating that depends on the task relevance of the visual stimuli. Crucially, this perceptual attentional gating can be identified both at the behavioral level, and on neuronal response profiles, these two measures highly correlating with each other from one session to the next. A very strong prediction is that the spatial extent of these filtering "in" and "out" filters is dynamically adjusted to trial difficulty and task contingencies.

Multiple Mechanisms of Distractor Suppression

Recent behavioral evidence has posited the existence of two distinct distractor suppression mechanisms, a proactive and a reactive suppression mechanism. During proactive suppression, the early perceptual processing of behaviorally irrelevant stimuli is suppressed. This type of suppression is coupled with a strong attentional enhancement of the perception of task relevant visual stimuli and can be viewed as a situation in which the visual system is tuned to maximize the response to expected task relevant items while ignoring all other visual items. In everyday life, this can come at a strong behavioral cost as task irrelevant items could still turn out to be behaviorally relevant. In contrast, reactive suppression would correspond to a situation in which the visual system does perceptually process task irrelevant items, and only subsequently suppress the build-up of goal-directed responses toward these irrelevant stimuli. The coupling between these two distinct mechanisms is thus theoretically crucial for a flexible adjustment to both behavioral demands and environmental constraints. Here, we provide the very first evidence for distinct neuronal mechanisms implementing proactive and reactive sensory suppression mechanisms.

Task-Relevant Distractors Are Suppressed Proactively

Several previous reports show that the successful rejection of task relevant distractors is associated with a low neuronal response to their onset (Schall et al. 1995; Suzuki and Gottlieb 2013; Cosman et al. 2018). In contrast, the attentional capture of such distractors and the production of a goal directed behavior

toward them is associated with a strong neuronal response to their onset. We reproduce these behavioral and neuronal observations. As discussed above, we further demonstrate that attentional capture is fully dependent on the locus of the attentional spotlight, which implements a filtering "in" function of task-relevant distractors. In other words, successful proactive distractor suppression is associated with trials in which the attentional spotlight is far away from the task-relevant distractor. We show that both FEF multi-unit activity and local field potentials (LFPs) are suppressed following task-relevant distractor presentation when behaviorally suppressed, but not when erroneously selected. Cosman et al. (2018) demonstrate that distractor suppression arises in the FEF prior to the occipital cortex. This would suggest that proactive distractor suppression is either implemented in the FEF or in an up-stream prefrontal area such as the dorsolateral prefrontal cortex. Given the fact that the FEF is at the source of attention control signals (Thompson 2005; Wardrak et al. 2006; Buschman and Miller 2009; Gottlieb 2012), the tight link we demonstrate between proactive distractor suppression and the spatial position of the attentional spotlight strongly suggests that proactive distractor suppression is implemented within the FEF.

Irrelevant Distractors Are Suppressed Reactively

Neuronal evidence of attentional reactive suppression is to the best of our knowledge sparse if not inexistent. Here, we show that task irrelevant distractor presentation correlates with a marked phasic response in the FEF multi-unit activity as well as with a marked visual evoked potential in the FEF LFPs; this whether the stimulus is correctly rejected or erroneously selected by the monkeys. Given the fact that visual evoked responses in the FEF are often taken as a signature of conscious perception (Thompson and Schall 1999, 2000; Libedinsky and Livingstone 2011; Panagiotaropoulos et al. 2012; van Vugt et al. 2018), one can hypothesize that both correctly rejected and erroneously selected task irrelevant distractors are perceived by the monkey. This is in contrast with correctly rejected task relevant distractors that have only a weak trace in the FEF multi-unit activity and LFPs and are thus most likely not perceived. However, as described above, the perceptual component of the irrelevant information is under the influence of a filtering "out" process centered onto the attentional spotlight. The multi-unit activity of correctly rejected task irrelevant distractors is then rapidly suppressed following the initial visually evoked response. This neuronal suppression is not present in the erroneously selected distractors and is taken as a neuronal signature of reactive distractor suppression and is compatible with a signal interrupting the ongoing perceptual and decision-making neural processes (Geng 2014; Marini et al. 2016; Chelazzi et al. 2019). Thus, reactive distractor suppression involves both an AS-based filtering "out" perceptual neuronal component as well as a neuronal suppressive component.

Interaction between Neuronal Reactive Suppression, Priority Map, and Attentional Spotlight Position in Space

An important question is how much this later neuronal suppressive component depends on the spatial priority map and the attentional spotlight as described for the perceptual component. The initial evoked response to the task irrelevant distractor is stronger as the distractors are presented closer and closer to the expected target location. Except for the condition in which distractors are displayed very close to the target (within 3°), the neuronal reactive suppression brings all these neuronal activities to a same threshold. The net result of this is that reactive suppression follows the task-based learned spatial priority map and is stronger for stimuli closer to the expected target location. Reactive suppression in the FEF can thus be implemented either by a suppression command that is proportional to the initial evoked response or by a command that brings down neuronal responses to a same threshold irrespective of the initial visual evoked response to the distractor. This is discussed next.

However, very close to the expected target location (within 3°), task irrelevant distractor suppression is weaker than for distractors presented between 3° and 6° of eccentricity from the expected target location. This is possibly due to the fact that in this specific region of the visual field, distinguishing between the target and the task irrelevant distractors is more difficult (Dent et al. 2012; Suzuki and Gottlieb 2013; Geng 2014). In our task, target and distractors shared the same features and contrast with respect to the background. Discriminating between the two is thus expected to involve a precise evaluation of their spatial contingencies and is expected to be enhanced by the attentional spotlight (Treisman and Gelade 1980; Duncan and Humphreys 1989; Wolfe and Horowitz 2004; Navalpakkam and Itti 2007; Goldstone et al. 2012; Lau et al. 2019; Lu et al. 2019). Confirming this view, the initial visual evoked response to the task-irrelevant distractor is enhanced when the attentional spotlight is close to it, while, at the same time, the extent to which the neuronal activity is suppressed is critical. The net effect of this is a markedly stronger neuronal reactive suppression at the heart of the attentional spotlight as compared with further away from it.

As discussed above, our results suggest that reactive suppressive component is most marked at the center of the attentional spotlight. This result is confirmed both at neural and at behavioral level, supporting a functional link between FEF and overt behavior. However, as originally proposed by Castiello and Umiltà (1992), the attentional spotlight is highly task dependent adapting its size to the target dimensions and on the number of task relevant objects in the scene (Ben Hamed et al. 2002; Womelsdorf et al. 2006; Niebergall et al. 2011), impacting space perception at a distance from the attentional focus (Wardak et al. 2011). For example, Ben Hamed et al. (2002) show that receptive field size of lateral intraparietal area neurons varies as a function of attentional load, Womelsdorf et al. (2006) show that receptive fields of middle temporal area MT shift as a function of spatial attention orientation, and Niebergall et al. (2011) suggest that the receptive field size of MT adapt so as to include all task-relevant objects. This might also be the case in the FEF. As a result, reactive suppression might encompass small or larger portions of the attentional spotlight depending on the task. Further investigations are needed.

One or Multiple Attentional Spotlights

The possibility of a split of AS, and thus of multiple attentional spotlights, has been initially proposed by Castiello and Umiltà (1992), and more recently supported by event-related potentials, functional magnetic resonance imaging and monkey single cell recording studies (Müller et al. 2003; McMains and Somers 2004; Morawetz et al. 2007; Drew et al. 2009; Niebergall et al. 2011). A major assumption of our current decoding approach is that subjects deploy a unique attentional spotlight rather than multiple spotlights, whereby for example, they would split their attention between the cued landmark (to select the target when

presented) and the uncued landmarks (suppress D distractors when presented). Given the structure of this decoder and while we are interpreting decoder output as the location of a unique spotlight, it could alternatively be interpreted as the location of the dominant attentional spotlight. In other words, when we decode the attentional spotlight say close to the ipsilateral landmark to the cued landmark, it could still be that a second spotlight, of lesser strength is still present at the cued location. This could be tested by tracking *d* distractor suppression for a given attention to target distance. Under such a hypothesis, the multiple spotlight framework would, for example, predict that distractor suppression is strong both at the locus of attention and at the locus of the cued landmark.

In the specific context of our task, one could further predict that only the attentional spotlight that is not anchored at the cued landmark is dynamic as described in Gaillard et al. (2020), see also Gaillard and Hamed 2020 and Amengual and Hamed 2021), while the attentional spotlight placed at the cued landmark is stable and would represent what we call here the priority map defined by task structure. This is actually a very appealing possibility in the sense that not only does it allow for the possibility of multiple attentional spotlights but also for multiple type of priority maps defined either by top-down cognitive contingencies or by bottom-up contingencies implemented through learning. The data presented in the present manuscript actually speak for both possibilities. Further experiments are required for a dissociation between these two possibilities, as well as, more generally speaking to test the hypothesis of dynamic multiple attentional spotlights.

Overall, our results indicate that the FEF plays a central role in stimulus selection and both reactive and proactive distractor suppression. These processes are modulated by both long-term learned spatial task contingencies as well as by the dynamic attentional exploration and exploitation of the visual field. How the different FEF neuronal functional subtypes contribute to these processes and how these processes are implemented at the whole brain level will need to be further explored.

Supplementary Material

Supplementary material can be found at *Cerebral Cortex* online.

Funding

S.B.H. was supported by ANR-11-BSV4–0011 & ANR-14-ASTR-0011-01, LABEX CORTEX funding (ANR-11-LABX-0042) from the Université de Lyon, within the program Investissements d'Avenir (ANR-11-IDEX-0007) operated by the French National Research Agency (ANR). We thank research engineer Serge Pinède for technical support and Jean-Luc Charieau and Fidji Francioly for animal care. All procedures were approved by the local animal care committee (C2EA42–13-02-0401-01) and the Ministry of research, in compliance with the European Community Council, Directive 2010/63/UE on Animal Care.

Notes

Conceptualization, S.B.H., F.D.B., and E.A.; Methodology, S.B.H., S.B.H.H., E.A., and F.D.B.; Investigation, S.B.H., S.B.H.H., E.A., and F.D.B.; Writing—Original Draft, S.B.H. and F.D.B.; Writing—Review & Editing, S.B.H. and F.D.B.; Funding Acquisition, S.B.H.; Supervision, S.B.H. No conflicts of interest are declared. We are grateful to Jean-Luc Charieau and Fidji Francioly for animal care, Serge Pinède for engineering support, and Johan Pacquit and Sylvain Maurin for informatics assistance. *Conflict of interest*. None.

References

Amengual JL, Hamed SB. 2021. Revisiting persistent neuronal activity during covert spatial attention. *Front Neural Circuits*. 15:60.

Anderson BA, Britton MK. 2020. On the automaticity of attentional orienting to threatening stimuli. *Emotion*. 20(6):1109.

Armstrong KM, Chang MH, Moore T. 2009. Selection and maintenance of spatial information by frontal eye field neurons. *J Neurosci*. 29(50):15621–15629. https://doi.org/10.1523/JNEUROSCI.4465-09.2009.

Astrand E, Enel P, Ibos G, Dominey PF, Baraduc P, Ben Hamed S. 2014. Comparison of classifiers for decoding sensory and cognitive information from prefrontal neuronal populations. edited by T. Boraud. *PLoS One*. 9(1):e86314. https://doi.org/10.1371/journal.pone.0086314.

Astrand E, Ibos G, Duhamel J-R, Ben Hamed S. 2015. Differential dynamics of spatial attention, position, and color coding within the parietofrontal network. *J Neurosci*. 35:3174–3189. https://doi.org/10.1523/JNEUROSCI.2370-14.2015.

Astrand E, Wardak C, Baraduc P, Ben Hamed S. 2016. Direct two-dimensional access to the spatial location of covert attention in macaque prefrontal cortex. *Curr Biol*. 26:1699–1704. https://doi.org/10.1016/j.cub.2016.04.054.

Astrand E, Wardak C, Ben Hamed S. 2014. Selective visual attention to drive cognitive brainâ€ machine interfaces: from concepts to neurofeedback and rehabilitation applications. *Front Syst Neurosci*. 8. https://doi.org/10.3389/fnsys.2014.00144.

Astrand E. 2018. A continuous time-resolved measure decoded from EEG oscillatory activity predicts working memory task performance. *J Neural Eng*. 15(3):036021. https://doi.org/10.1088/1741-2552/aaae73.

Astrand E, Wardak C, Hamed SB. 2020. Neuronal population correlates of target selection and distractor filtering. *NeuroImage*. 209:116517. https//doi.org/10.1016/j.neuroimage.2020.116517.

Awh E, Belopolsky AV, Theeuwes J. 2012. Top-down versus bottom-up attentional control: a failed theoretical dichotomy. *Trends Cogn Sci*. 16(8):437–443. https://doi.org/10.1016/j.tics.2012.06.010.

Baluch F, Itti L. 2011. Mechanisms of top-down attention. *Trends Neurosci*. 34(4):210–224. https://doi.org/10.1016/j.tins.2011.02.003.

Di Bello, F, Giamundo, M, Brunamonti E, Cirillo R, Ferraina S. 2019. The puzzling relationship between attention and motivation: do Motor biases matter? *Neuroscience*. 406:150–158.

Ben Hamed S, Duhamel JR, Bremmer F, Graf W. 2002. Visual receptive field modulation in the lateral intraparietal area during attentive fixation and free gaze. *Cereb Cortex*. 12(3):234–245.

Bettencourt KC, Somers DC. 2009. Effects of target enhancement and distractor suppression on multiple object tracking capacity. *J Vis*. 9(7):9–9. https://doi.org/10.1167/9.7.9.

Buschman TJ, Miller EK. 2009. Serial, covert shifts of attention during visual search are ref lected by the frontal eye fields and correlated with population oscillations. *Neuron*. 63(3):386–396. https://doi.org/10.1016/j.neuron.2009.06.020.

Carrasco M, Frieder KS. 1997. Cortical magnification neutralizes the eccentricity effect in visual search. *Vis Res*. 37(1):63–82. 10.1016/S0042-6989(96)00102-2.

Castiello U, Umiltà C. 1992. Splitting focal attention. *J Exp Psychol Hum Percept Perform*. 18(3):837–848. https//doi.org/10.1037/0096-1523.18.3.837.

Chelazzi L, Marini F, Pascucci D, Turatto M. 2019. Getting rid of visual distractors: the why, when, how, and where. *Curr Opin Psychol*. 29:135–147. https://doi.org/10.1016/j.copsyc.2019.02.004.

Chelazzi L, Perlato A, Santandrea E, Della Libera C. 2013. Rewards teach visual selective attention. *Vis Res*. 85:58–72. https://doi.org/10.1016/j.visres.2012.12.005.

Chelazzi L, J. E To inova, Calletti R, Gerfo EL, Sani I, Libera CD, Santandrea E. 2014. Altering spatial priority maps via reward-based learning. *J Neurosci*. 34(25):8594–8604. https://doi.org/10.1523/JNEUROSCI.0277-14.2014.

Chica AB, Martín-Arévalo E, Botta F, Lupiáñez J. 2014. The spatial orienting paradigm: how to design and interpret spatial attention experiments. *Neurosci Biobehav Rev*. 40:35–51. https://doi.org/10.1016/j.neubiorev.2014.01.002.

Choi I, Kurozumi E. 2012. Model selection criteria for the leads-and-lags cointegrating regression. *J Econ*. 169:224–238.

Corbetta M, Patel G, Shulman GL. 2008. The reorienting system of the human brain: from environment to theory of mind. *Neuron*. 58(3):306–324.

Cosman JD, Lowe KA, Zinke W, Woodman GF, Schall JD. 2018. Prefrontal control of visual distraction. *Curr Biol*. 28:414–420e3. https://doi.org/10.1016/j.cub.2017.12.023.

Della Libera C, Chelazzi L. 2009. Learning to attend and to ignore is a matter of gains and losses. *Psychol Sci*. 20:778–784. https://doi.org/10.1111/j.1467-9280.2009.02360.x.

Demeter E, Hernandez-Garcia L, Sarter M, Lustig C. 2011. Challenges to attention: a continuous arterial spin labeling (ASL) study of the effects of distraction on sustained attention. *NeuroImage*. 54(2):1518–1529.

Dent K, Allen HA, Braithwaite JJ, Humphreys GW. 2012. Parallel distractor rejection as a binding mechanism in search. *Front Psychol*. 3:278. https://doi.org/10.3389/fpsyg.2012.00278.

Desimone R, Duncan J. 1995. Neural mechanisms of selective visual attention. *Annu Rev Neurosci*. 18:193–222. https://doi.org/10.1146/annurev.ne.18.030195.001205.

Doricchi F, Merola S, Aiello M, Guariglia P, Bruschini M, Gevers W, Gasparini M, Tomaiuolo F. 2009. Spatial orienting biases in the decimal numeral system. *Curr Biol*. 19(8):682–687.

Downing CJ, Pinker S. 1985. The spatial structure of visual attention. Pp. 171–87 in *Attention and Performance XI: Mechanisms of attention and visual search*. Hillsdale, NJ: Erlbaum.

Drew T, McCollough AW, Horowitz TS, Vogel EK. 2009. Attentional enhancement during multiple-object tracking. *Psychon Bull Rev*. 16(2):411–417.

Duncan J, Humphreys GW. 1989. Visual search and stimulus similarity. *Psychol Rev*. 96(3):433–458. https://doi.org/10.1037/0033-295x.96.3.433.

Durston S, Tottenham NT, Thomas KM, Davidson MC, Eigsti I-M, Yang Y, Ulug AM, Casey BJ. 2003. Differential patterns of striatal activation in young children with and without ADHD. *Biol Psychiatry*. 53(10):871–878.

Einevoll GT, Kayser C, Logothetis NK, Panzeri S. 2013. Modelling and analysis of local field potentials for studying the function of cortical circuits. *Nat Rev Neurosci*. 14:770–785. https://doi.org/10.1038/nrn3599.

Farbod Kia S, Åstrand E, Ibos G, Ben Hamed S. 2011. Read-out of the intrinsic and extrinsic properties of a stimulus from un-experienced neuronal activities: towards cognitive neuroprostheses. *J Physiol Paris*. 105:115–122. https://doi.org/10.1016/j.jphysparis.2011.07.015.

Ferrante O, Patacca A, Di Caro V, Libera CD, Santandrea E, Chelazzi L. 2018. Altering spatial priority maps via statistical learning of target selection and distractor filtering. *Cortex*. 102:67–95. https://doi.org/10.1016/j.cortex.2017.09.027.

Fiebelkorn IC, Saalmann YB, Kastner S. 2013. Rhythmic sampling within and between objects despite sustained attention at a cued location. *Curr Biol*. 23:2553–2558. https://doi.org/10.1016/j.cub.2013.10.063.

Fiebelkorn IC, Kastner S. 2019. A rhythmic theory of attention. *Trends Cogn Sci*. 23(2):87–101. https://doi.org/10.1016/j.tics.2018.11.009.

Fiebelkorn IC, Pinsk MA, Kastner S. 2018. Dynamic interplay within the frontoparietal network underlies rhythmic spatial attention. *Neuron*. 99(4):842–853.e8. https://doi.org/10.1016/j.neuron.2018.07.038.

Gaillard C, Hamed SB. 2020. The neural bases of spatial attention and perceptual rhythms. *Eur J Neurosci*. ejn.15044. https://doi.org/10.1111/ejn.15044.

Gaillard C, Hassen SBH, Di Bello F, Bihan-Poudec Y, Van-Rullen R, Hamed SB. 2020. Prefrontal attentional saccades explore space rhythmically. *Nat Commun*. 11(1):925. https://doi.org/10.1038/s41467-020-14649-7.

Gaspelin N, Leonard CJ, Luck SJ. 2015. Direct evidence for active suppression of salient-but-irrelevant sensory inputs. *Psychol Sci*. 26(11):1740–1750. https://doi.org/10.1177/0956797615597913.

Geng JJ. 2014. Attentional mechanisms of distractor suppression. *Curr Dir Psychol Sci*. 23:147–153. https://doi.org/10.1177/0963721414525780.

Gilbert CD, Wu L. 2013. Top-down influences on visual processing. *Nat Rev Neurosci*. 14(5):350–363. https://doi.org/10.1038/nrn3476.

Gottlieb J. 2012. Attention, learning, and the value of information. *Neuron*. 76(2):281–295. https://doi.org/10.1016/j.neuron.2012.09.034.

Gregoriou GG, Gotts SJ, Zhou H, Desimone R. 2009. High-frequency, long-range coupling between prefrontal and visual cortex during attention. *Science (New York, N.Y.)*. 324(5931):1207–1210. https://doi.org/10.1126/science.1171402.

Hasegawa RP, Peterson BW, Goldberg ME. 2004. Prefrontal neurons coding suppression of specific saccades. *Neuron*. 43:415–425. https://doi.org/10.1016/j.neuron.2004.07.013.

Hembrook-Short JR, Mock VL, Usrey WM, Briggs F. 2019. Attention enhances the efficacy of communication in V1 local circuits. *J Neurosci*. 39:1066–1076. https://doi.org/10.1523/JNEUROSCI.2164-18.2018.

Hickey C, Di Lollo V, McDonald JJ. 2009. Electrophysiological indices of target and distractor processing in visual search. *J Cogn Neurosci*. 21(4):760–775.

Hopf J-M, Boehler CN, Schoenfeld MA, Heinze H-J, Tsotsos JK. 2010. The spatial profile of the focus of attention in visual search: insights from MEG recordings. *Vis Res*. 50:1312–1320. https://doi.org/10.1016/j.visres.2010.01.015.

Ibos G, Duhamel J-R, Ben Hamed S. 2013. A functional hierarchy within the parietofrontal network in stimulus selection and attention control. *J Neurosci*. 33:8359–8369. https://doi.org/10.1523/JNEUROSCI.4058-12.2013.

James W. 1890. *The Principles of Psychology*. New York: Holt.

Jiang, Yuhong V., Li Z. Sha, and Caitlin A. Sisk. 2018. Experience-Guided Attention: Uniform and Implicit. *Attention, Perception & Psychophysics*. 80(7):1647–53. https://doi.org/10.3758/s13414-018-1585-9.

Landau AN, Fries P. 2012. Attention samples stimuli rhythmically. *Curr Biol*. 22:1000–1004. https://doi.org/10.1016/j.cub.2012.03.054.

Lau JS-H, Pashler H, Brady TF. 2019. Target templates in low target-distractor discriminability visual search have higher resolution, but the advantage they provide is short-lived. Preprint. *PsyArXiv*. https://doi.org/10.31234/osf.io/ab8h2.

Leber AB. 2010. Neural predictors of within-subject fluctuations in attentional control. *J Neurosci*. 30(34):11458–11465. https://doi.org/10.1523/JNEUROSCI.0809-10.2010.

Li S, Remington R, Jiang Y. 2018. Learning-induced changes in attentional priority map are task-specific. *J Vis*. 18(10):1182–1182.

Libedinsky C, Livingstone M. 2011. Role of prefrontal cortex in conscious visual perception. *J Neurosci*. 31(1):64–69. https://doi.org/10.1523/JNEUROSCI.3620-10.2011.

Lu VT, Wright CE, Chubb C, Sperling G. 2019. Variation in target and distractor heterogeneity impacts performance in the centroid task. *J Vis*. 19(4):21. https://doi.org/10.1167/19.4.21.

Marini F, Demeter E, Roberts KC, Chelazzi L, Woldorff MG. 2016. Orchestrating proactive and reactive mechanisms for filtering distracting information: brain-behavior relationships revealed by a mixed-design fMRI study. *J Neurosci*. 36:988–1000. https://doi.org/10.1523/JNEUROSCI.2966-15.2016.

McMains SA, Somers DC. 2004. Multiple spotlights of attentional selection in human visual cortex. *Neuron*. 42(4):677–686.

McManus JNJ, Wu L, Gilbert CD. 2011. Adaptive Shape Processing in Primary Visual Cortex. *Proceedings of the National Academy of Sciences of the United States of America*. 108(24):9739–9746. https://doi.org/10.1073/pnas.1105855108.

Monosov IE, Trageser JC, Thompson KG. 2008. Measurements of simultaneously recorded spiking activity and local field potentials suggest that spatial selection emerges in the frontal eye field. *Neuron*. 57:614–625. https://doi.org/10.1016/j.neuron.2007.12.030.

Morawetz C, Holz P, Baudewig J, Treue S, Dechent P. 2007. Split of attentional resources in human visual cortex. *Vis Neurosci*. 24(6):817–826.

Moore T, Fallah M. 2001. Control of Eye Movements and Spatial Attention. *Proceedings of the National Academy of Sciences of the United States of America*. 98(3):1273–1276. https://doi.org/10.1073/pnas.021549498.

Moore T, Zirnsak M. 2017. Neural Mechanisms of Selective Visual Attention. *Annual Review of Psychology*. 68:47–72. https://doi.org/10.1146/annurev-psych-122414-033400.

Müller MM, Malinowski P, Gruber T, Hillyard SA. 2003. Sustained division of the attentional spotlight. *Nature*. 424(6946):309–312.

Navalpakkam V, Itti L. 2007. Search Goal Tunes Visual Features Optimally. *Neuron*. 53(4):605–617. https://doi.org/10.1016/j.neuron.2007.01.018.

Niebergall R, Khayat PS, Treue S, Martinez-Trujillo JC. 2011. Multifocal attention filters targets from distracters within and beyond primate MT neurons' receptive field boundaries. *Neuron*. 72(6):1067–1079.

Nielsen KJ, Logothetis NK, Rainer G. 2006. Dissociation between local field potentials and spiking activity in macaque inferior temporal cortex reveals diagnosticity-based encoding of complex objects. *J Neurosci*. 26:9639–9645. https://doi.org/10.1523/JNEUROSCI.2273-06.2006.

Nobre K, Kastner S, editors. 2014. *The Oxford Handbook of Attention. Oxford*. New York: Oxford University Press.

Noudoost B, Chang MH, Steinmetz NA, Moore T. 2010. Top-down control of visual attention. *Curr Opin Neurobiol*. 20:183–190. https://doi.org/10.1016/j.conb.2010.02.003.

Panagiotaropoulos TI, Deco G, Kapoor V, Logothetis NK. 2012. Neuronal Discharges and Gamma Oscillations Explicitly Reflect Visual Consciousness in the Lateral Prefrontal Cortex. *Neuron*. 74(5):924–935. https://doi.org/10.1016/j.neuron.2012.04.013.

Perri RL. 2019. Is there a proactive and a reactive mechanism of inhibition? Towards an executive account of the attentional inhibitory control model. *Behav Brain Res*. 377:112243.

Posner MI. 1980. Orienting of attention. Q *J Exp Psychol (Hove)*. 32(1):3–25. https://doi.org/10.1080/00335558008248231.

Schwartz EL. 1994. Computational Studies of the Spatial Architecture of Primate Visual Cortex. In: *Primary visual cortex in primates*. Springer, pp. 359–411.

Sousa D, Carine CG, Di Bello C, Hassen FBH, Ben Hamed S. 2021. Behavioral validation of novel high resolution attention decoding method from multi-units & local field potentials. *NeuroImage*. 231:117853.

Spyropoulos G, Bosman CA, Fries P. 2018. A theta rhythm in macaque visual cortex and its attentional modulation. *Proc Natl Acad Sci USA*. 115:E5614–E5623. https://doi.org/10.1073/pnas.1719433115.

Squire RF, Noudoost B, Schafer RJ, Moore T. 2013. Prefrontal contributions to visual selective attention. *Annu Rev Neurosci*. 36:451–466. https://doi.org/10.1146/annurev-neuro-062111-150439.

Suzuki M, Gottlieb J. 2013. Distinct neural mechanisms of distractor suppression in the frontal and parietal lobe. *Nat Neurosci*. 16:98–104. https://doi.org/10.1038/nn.3282.

Theeuwes J. 2010. Top-down and bottom-up control of visual selection: reply to commentaries. *Acta Psychol*. 135:133–139. https://doi.org/10.1016/j.actpsy.2010.07.006.

Thompson KG, Schall JD. 2000. Antecedents and Correlates of Visual Detection and Awareness in Macaque Prefrontal Cortex. *Vision Research*. 40(10–12):1523–1538. https://doi.org/10.1016/s0042-6989(99)00250-3.

Thompson KG. 2005. Neuronal basis of covert spatial attention in the frontal eye field. *J Neurosci*. 25:9479–9487. https://doi.org/10.1523/JNEUROSCI.0741-05.2005.

Thompson KG, Bichot NP. 2005. A visual salience map in the primate frontal eye field. *Prog Brain Res*. 147:251–262.

Thompson KG, Bichot NP, Schall JD. 1997. Dissociation of visual discrimination from saccade programming in macaque frontal eye field. *J Neurophysiol*. 77:1046–1050. https://doi.org/10.1152/jn.1997.77.2.1046.

Treisman AM, Gelade G. 1980. A Feature-Integration Theory of Attention. *Cognitive Psychology*. 12(1):97–136. https://doi.org/10.1016/0010-0285(80)90005-5.

van Vugt B, Dagnino B, Vartak D, Safaai H, Panzeri S, Dehaene S, Roelfsema PR. 2018. The threshold for conscious report: signal loss and response bias in visual and frontal cortex. *Science*. 360:537–542. https://doi.org/10.1126/science.aar7186.

Vissers ME, van Driel J, Slagter HA. 2016. Proactive, but not reactive, distractor filtering relies on local modulation of alpha oscillatory activity. *J Cogn Neurosci*. 28(12):1964–1979.

Wager TD, Sylvester C-YC, Lacey SC, Nee DE, Franklin M, Jonides J. 2005. Common and unique components of response inhibition revealed by FMRI. *NeuroImage*. 27(2):323–340.

Wardak C, Ibos G, Duhamel J-R, Olivier E. 2006. Contribution of the monkey frontal eye field to covert visual attention. *J Neurosci*. 26(16):4228–4235. https://doi.org/10.1523/JNEUROSCI.3336-05.2006.

Wardak C, Denève S, Hamed SB. 2011. Focused visual attention distorts distance perception away from the attentional locus. *Neuropsychologia*. 49(3):535–545. https://doi.org/10.1016/j.neuropsychologia.2010.12.008.

Wolfe JM, Horowitz TS. 2004. What attributes guide the deployment of visual attention and how do they do it? Nature reviews. *Neuroscience*. 5(6):495–501. https://doi.org/10.1038/nrn1411.

Womelsdorf T, Anton-Erxleben K, Pieper F, Treue S. 2006. Dynamic shifts of visual receptive fields in cortical area MT by spatial attention. *Nat Neurosci*. 9(9):1156–1160.

You L, Li Z, Huang J, Du A. 2016. The Tikhonov regularization method in Hilbert scales for determining the unknown source for the modified Helmholtz equation. *JAMP*. 04:140–148. https://doi.org/10.4236/jamp.2016.41017.